astronomy

MDPI

Article

RisingTides: An Analytic Modeling Code of Tidal Effects in Binary Neutron Star Mergers

Alexander O'Dell † and Maria C. Babiuc Hamilton *,†

Department of Physics, Marshall University, 1 John Marshall Drive, Huntington, WV 25755, USA; odell97@marshall.edu

* Correspondence: babiuc@marshall.edu

† These authors contributed equally to this work.

Abstract: Gravitational waves produced by binary neutron star mergers offer a unique window into matter behavior under extreme conditions. In this context, we analytically model the effect of matter on gravitational waves from binary neutron star mergers. We start with a binary black hole system, leveraging the post-Newtonian formalism for the inspiral and the Backwards-one-Body model for the merger. We combine the two methods to generate a baseline waveform and we validate our results against numerical relativity simulations. Next, we integrate tidal effects in phase and amplitude to account for matter and spacetime interaction using the NRTidal model and test its accuracy against numerical relativity predictions for two equations of state, finding a mismatch around the merger. Subsequently, we lift the restriction on the coefficients to be independent of the tidal deformability and recalibrate them using the numerical relativity predictions. We obtain better fits for phase and amplitude around the merger and are able to extend the phase modeling beyond the merger. We implement our method in new open-source, user-friendly Python code, steered by a Jupyter Notebook, named RisingTides. Our research offers new perspectives on analytically modeling the effect of tides on the gravitational waves from binary neutron star mergers.

Keywords: binary neutron star mergers; analytical modeling; gravitational waves; tidal deformability

Citation: O'Dell, A.; Hamilton, M.C.B. RisingTides: An Analytic Modeling Code of Tidal Effects in Binary Neutron Star Mergers. *Astronomy* **2024**, *3*, 167–188. https://doi.org/10.3390/astronomy3030011

Academic Editor: Ignatios Antoniadis

Received: 31 May 2024
Revised: 20 June 2024
Accepted: 25 June 2024
Published: 2 July 2024

1. Introduction

Neutron stars are extremely dense remnants of massive stars at the brink of collapsing into a black hole, with masses comparable to that of the sun contained in only twenty kilometers diameter. They are captivating celestial objects under the action of powerful gravitational and magnetic fields, which cannot be replicated on Earth. These exceptional properties present them as excellent astrophysical laboratories for investigating the behavior of matter in extreme conditions of density, pressure, and temperature. When two neutron stars collide and merge, they emit gravitational waves, accompanied by electromagnetic radiation, matter, and neutrinos, carrying valuable information about their masses, sizes, and interior structure.

The first direct detection of a gravitational wave (GW) signal from a binary neutron star (BNS) collision, named GW170817 [1], was accompanied by a gamma-ray burst [2] and ignited a new explosion, called a kilonova, powered by the radioactive decay of the heavy elements synthesized in the merger [3]. This twin detection marked the onset of the golden era in neutron star research, alluding to the precious metals such as gold synthesized and expelled during the collision and has inspired intense theoretical investigations. These studies provided us with a wealth of new insights into the yet unknown internal structure of neutron stars [4–6], the characteristics of their magnetic fields [7], and the outflow of heavy matter during collision [8].

Unfortunately, simultaneous detections of gravitational waves and light are few and far between. Out of the almost 100 such events reported to date [9], the overwhelming majority

came from binary black hole (BBH) collisions and only one other, named GW190425, was produced by an unusually heavy BNS collision [10,11]. The two BNS mergers detected so far have raised many questions, proving again that nature is more complicated than our models [12,13]. It is thus imperative to revise our current understanding of the physics involved in those models in order to gain insight on BNS mergers. This is a timely topic because in the next decade, hundreds of such GW events might be detected [14] with the advent of the new generation of gravitational wave observatories, including both ground-based detectors such as Cosmic Explorer [15] and the Einstein Telescope [16] and space-borne instruments such as LISA [17], DECIGO [18], and TianQin [19].

Efforts in the analytical modeling of the tidal interactions during BNS mergers have focused on developing post-Newtonian (pN) approximations for the late-inspiral phase [20–23], relying on the effective-one-body (EOB) approach [24–27]. As those approximations become less accurate near merger [28–30], alternative methods have emerged, notably the closed-form tidal approximants [31–36], which combine pN, tidal EOB, and numerical relativity (NR) data.

In this study, we employ the NRTidal approximant [31,33,34], an elegant model that adjusts the analytically calculated BBH waveforms by adding a closed-form expression to account for the tidal influences in the phase and amplitude of the GW. This model was used for estimating source properties [37] and constraining the equation of state for ultra-dense matter in the first two BNS detections [38], and it is implemented in the LIGO Scientific and Virgo Collaborations Algorithm Library Suite (LALSuite) [39].

Our goal is to analytically model the effect of tides on the GW signal during the inspiral of a BNS system and assess the quality of the implementation of tidal effects described by the analytical NRTidal model against NR datasets that were not used in the initial calibration. We also aim to accurately extend it through the merger of the BNS systems considered by introducing a novel approach to analytically model the effects of tides around the merger, thus obtaining a comprehensive modeling of tidal effects throughout both the inspiral and merger phases. We create a new open-source, user-friendly, easily replicable code RisingTides and use it to generate comprehensive analytical templates for gravitational radiation during BNS collisions. In terms of accuracy, our GW signal templates show a high degree of consistency with the numerical simulations considered. By presenting our analytical model and the open-source code, we provide the scientific community with a powerful and accessible tool for advancing the understanding of these complex phenomena, especially for students and researchers who enter the field or who need to explore the parameter space and generate reliable results quickly. Our motivation in releasing RisingTides is to broaden participation in GW research and also to enhance reproducibility and collaborative efforts. By doing so, we facilitate independent consistency checks and assist in defining the domains of validity for the approximation models employed. Ultimately, our work contributes to the development of a universal analytical model encapsulating the BNS dynamics and the effect of tides on GW emission.

This paper unfolds as follows: First, we present the point-particle system that characterizes BBH collisions and calculate the GW by combining the pN formalism for inspiral evolution with the Backwards-one-Body (BoB) model for the merger. As a baseline GW, we use the fully analytical model for BBH collision we developed in [40] and expanded in [41] based on [42] for the inspiral and [43] for the merger. We prove our model's validity and efficiency through a comparison with NR, utilizing the `SXS:BBH:0180` template from the Simulating eXtreme Spacetimes (SXS) catalog [44]. We then incorporate the tidal deformability into the point-particle waveform, both as polynomial corrections and as rational functions approximations to the phase and amplitude by using the coefficients proposed in [33,34]. Next, we test our implementation against `SXS:NSNS:0001/0002` for two equations of state [45].

Finally, we push this model past the merger by performing a new fit to the numerical BNS data for the tidal phase and amplitude from which we derive updated values for the polynomial coefficients, thus expanding its applicability. Upon determining the new

coefficients, we reconstruct the tidal correction in phase and amplitude beyond the merger and analyze the tidal influence on the early stages of the collision, revealing the effect of the matter interaction on the system's orbits.

In this work, we consider two neutron stars with total mass $M = M_A + M_B$, $M_A \leq M_B$, and a mass ratio $q = M_B/M_A \geq 1$. We express time, space, and energy in geometric units (with $G = c = 1$), in terms of the binary mass M, written as a multiple of the sun mass $M_\odot$. Our implementation allows systems with unequal mass ratios; however, in this work we present results only for the equal-mass case.

2. Implementation of the Baseline Model

We start with assembling the baseline analytical model for the calculation of the GWs from a BBH collision by following a common procedure as we detailed in [40,41]. First, we split the binary motion in two regions—the weak field, during the inspiral and the strong field, during the merger—and apply different mathematical formalisms to obtain the waveform for each region. We then generate the complete GW template for the whole binary evolution by matching those two regions in frequency around the last stable orbit and building the hybrid waveform. Lastly, we compare our model against a numerically generated equal mass BBH collision to uphold its validity.

2.1. The Baseline Inspiral Model

Let us consider a tight binary system of separation r in a quasi-circular orbit. By defining the reduced mass $\mu = (M_A M_B)/M$ and the symmetric mass ratio $\eta = \mu/M$, we reduce it further to a single particle of mass μ and position r orbiting around the mass M located at the center of mass. We require the system to dissipate GWs and are led to following the balance equation:

$$F(t) = -\frac{dE(t)}{dt}. \tag{1}$$

This formula states that the GW flux $F(t)$ is emitted at the expense of the orbital energy $E(t)$, causing the orbit to shrink. Equation (1) can be rewritten in terms of a small factor $x_{pN} = (v/c)^2$ called the post-Newtonian parameter, where v is the orbital velocity of the binary and c is the speed of light (see [46–49]).

$$\frac{dx_{pN}(t)}{dt} = -\frac{F(t)}{dE(t)/dx_{pN}(t)}. \tag{2}$$

Using the pN approximation, we expand the deviation from Newtonian gravity as a perturbation in the power series of x_{pN}. From the many different methods of solving Equation (2), in this work we chose the TaylorT4 approximant, shown to agree best with numerical simulations [50]. Within this method, Equation (2) becomes [40,42]:

$$\left.\frac{dx_{pN}(t)}{dt}\right|^{\frac{N}{2}} = \frac{x_{pN}^5(t)}{M} \sum_{j=0}^{N} \xi_j x_{pN}^{j/2}(t). \tag{3}$$

where $N/2$ denotes the pN expansion order. In this work, we go up to 3.5 in the leading pN order, adding self-force and hereditary correction terms up to 6pN order to increase the accuracy in modeling the region near the merger [42]. By integrating Equation (3) with the coefficients ξ_j, we obtain the evolution of the pN parameter x_{pN}. Next, we use Kepler's third law $v^2 = (M\Omega(t))^{2/3}$ where Ω is the angular orbital velocity to obtain the equation for the orbital phase:

$$\frac{d\phi_{pN}(t)}{dt} = \Omega(t) = \frac{x_{pN}(t)^{3/2}}{M}. \tag{4}$$

We readily integrate Equation (4) to find the time evolution of the orbital inspiral phase.

We reuse Kepler's third law written as $v = \sqrt{M/r}$ to extract the orbital separation as $r = M/x_{pN}$, which we then expand in powers series of x_{pN} for increased accuracy:

$$r_{pN}(t) = \frac{M}{x_{pN}(t)} \sum_{j=0}^{3} \rho_j x_{pN}(t)^j. \tag{5}$$

Lastly, we calculate the GW amplitude for optimal orientation of the source,

$$A_{\mathcal{R}}(t) = -2\frac{\mu}{R}\left[\frac{M}{r_{pN}(t)} + r_{pN}(t)^2\left(\frac{d\phi_{pN}(t)}{dt}\right)^2 - \left(\frac{dr_{pN}(t)}{dt}\right)^2\right],$$
$$A_{\mathcal{I}}(t) = -4\frac{\mu}{R} r_{pN}(t)\frac{d\phi_{pN}(t)}{dt}\frac{dr_{pN}(t)}{dt}. \tag{6}$$

Now, we have all the pieces necessary to construct the dimensionless strain, defined as follows:

$$h_{pN}(t) = A_{pN}(t)e^{-2i\phi_{pN}(t)} \tag{7}$$

Mathematically, the strain is decomposed into two transverse *quadrupolar* polarization modes with h_+ representing the real part of Equation (7) and $h_\times$ the imaginary part,

$$h_{+,pN}(t) = A_{\mathcal{R}}(t)\cos(2\phi_{pN}) + iA_{\mathcal{I}}(t)\sin(2\phi_{pN}),$$
$$h_{\times,pN}(t) = A_{\mathcal{R}}(t)\sin(2\phi_{pN}) - iA_{\mathcal{I}}(t)\cos(2\phi_{pN}). \tag{8}$$

This is because the GWs compress the space in one direction while simultaneously stretching it in the orthogonal direction such that the signal goes twice through maxima and minima during one orbital cycle, making the frequency of the GW twice the orbital frequency. This technique, albeit powerful, is valid only if the gravitational field is sufficiently weak and the orbital velocity is smaller than the speed of light.

2.2. The Baseline Merger Model

Going beyond the pN approximation brings us up against the strong gravitational field around the merger. The transition between the weak and strong field is marked by the innermost stable circular orbit (ISCO), defined as the last stable orbit that a particle would have when orbiting around a black hole. When the masses of the celestial objects are comparable, this location is not well defined [51] but can be approximated with the last stable photon orbit, called the light ring (LR), which is close to the peak of the curvature potential [52]. The light ring (or the photon sphere) represents the orbit where the orbital velocity equals the speed of light (for a detailed discussion, see [53]). Its location plays an important role in determining the boundary between inspiral and merger, which is essential for the matching procedure [54].

From there on, through the merger and ringdown, we use the Backwards-one-Body (BoB) formalism [43]. This technique starts from the perturbed final black hole resulting after collision and builds the GW signal back in time to the end of the inspiral, assuming we know the mass, spin, and ringdown frequency of the remnant. In this model, the strain of the GW signal can be modeled analytically as exponentially decaying sinusoids that break free from the LR on null geodesics [55]:

$$h_{BoB}(t) = \sum_{lmn} A_{lmn} e^{it\left(\omega_{lmn} - \frac{1}{\tau_{lmn}}\right)}, \tag{9}$$

where l is the principal, $|m| \leq l$ the azimuthal, and n is the overtone index of a mode. This kind of perturbation is called *quasinormal* (QNM) ringing with frequency ω_{lmn} and damping time τ_{lmn}. The frequency of the lower mode is $(l = 2, m = 1, n = 0)$, coincides with the orbital frequency, and we will denote it as Ω_{QNM}. The $(l = 2, m = 2, n = 0)$ mode can be derived from this mode with the simple relation $\omega_{22} = 2\Omega_{QNM}$. This mode

carries away most of the GW's energy (≈95%) [56], while the higher harmonics, being much quieter, can be usually neglected. We will drop the (l, m, n) indices and consider that the strain is well described by the dominant mode.

The BoB model requires the QNM frequency and damping time, which are determined by the spin and mass of the final black hole. We will estimate the final spin of the resulting black hole with a polynomial of coefficients s_{ij}, as given in [57,58]:

$$\chi_f = \sum_{i,j=0}^{3} s_{ij} \eta^i \chi_{eff}^j. \tag{10}$$

We define an effective spin:

$$\chi_{eff} = \frac{M_A^2 \chi_A + M_B^2 \chi_B}{M_A^2 + M_B^2}, \tag{11}$$

with $\chi_{A,B} = S_{A,B}/M_{A,B}^2$ as the dimensionless individual spins and $S_{A,B}$ as the spin angular momentum of each black hole entering the merger. In our calculations, we choose $\chi_{A,B} = 0$, as in the NR simulations we use for comparison, although the mean spin for low-spinning astronomical neutron stars is $\chi_{A,B} \approx 2 \times 10^{-3}$ [59].

For the final mass, we use the fit to NR given in [60] for comparable mass binaries,

$$M_f = M(1 - \tilde{E}_{GW}) - M_{disk} \tag{12}$$

where $\tilde{E}_{GW} = E_0 + E_2 \chi_f^2 + E_4 \chi_f^4$ is the dimensionless energy released in GWs. For the disk mass, we take an upper limit of $M_{disk} \approx 10^{-2} M$ [61]. The coefficients for E_i are given in Table III of [60].

Next, we calculate the dominant resonant frequency with a polynomial fit:

$$M_f \Omega_{QNM} = f_1 + f_2 (1 - \chi_f)^{f_3}, \tag{13}$$

and use a similar formula for the quality factor:

$$Q = q_1 + q_2 (1 - \chi_f)^{q_3}. \tag{14}$$

The pairs (f_i, q_i) are taken from Table VIII of [56]. Lastly, the damping time is as follows:

$$\tau_{QNM} = \frac{2Q}{\omega_{QNM}}. \tag{15}$$

The orbital angular frequency $\Omega_{BoB}(t)$ is given in this model by a hyperbolic tangent describing the evolution of the orbital frequency during the merger and ringdown (see Equation (7) in [43]):

$$\Omega_{BoB}(t) = \left(\Omega_i^4 + \kappa \left[\tanh\left(\frac{t - t_0}{\tau} \right) - \tanh\left(\frac{t_i - t_0}{\tau} \right) \right] \right)^{1/4}. \tag{16}$$

Here, Ω_i is the initial frequency, t_0 is the time at which the strain of the GW reaches its peak amplitude, and t_i the initial time, marking the transition between the weak and strong regime. The parameter κ in Equation (16) assures continuity between the end of the inspiral and the beginning of the merger and is given by the following:

$$\kappa = \left[\frac{\Omega_{QNM}^4 - \Omega_i^4}{1 - \tanh\left(\frac{t_i - t_0}{\tau} \right)} \right]. \tag{17}$$

The essential variable in the BoB model is the initial time t_i, which locks in the frequency Ω_i at the beginning of the merger to the frequency at end of the inspiral:

$$t_i = t_0 - \frac{\tau}{2} \ln\left(\frac{\Omega_{QNM}^4 - \Omega_i^4}{2\tau\Omega_i^3\dot{\Omega}_i} - 1\right). \tag{18}$$

We obtain the phase $\phi_{BoB}(t)$ by integrating Equation (16) between t_i and a final time t_f:

$$\phi_{BoB}(t) = \int_{t_i}^{t_f} \Omega_{BoB}(t) dt. \tag{19}$$

The amplitude of the GW signal is modeled with a simple function (see Equation (5) of [43]):

$$A_{BoB}(t) = A_0 \mathrm{sech}\left(\frac{t - t_0}{\tau}\right), \tag{20}$$

where A_0 is a scaling factor. This amplitude is taken to correspond to the Weyl scalar $|\Psi_4(t)|$, which is related to the strain by the formula

$$\Psi_4(t) = \frac{\partial^2 h_{GW}(t)}{\partial t^2}. \tag{21}$$

The model rests upon the assumption that the amplitude changes much slower compared to the phase during the merger and uses the simple expression for the strain given by Equation (32) in [62]:

$$h_{BoB}(t) = -\frac{A_{BoB}(t)}{\omega_{BoB}(t)^2} e^{-2i\phi_{BoB}(t)}, \tag{22}$$

where $\omega_{BoB}(t) = 2\Omega_{BoB}(t)$ is the frequency of the dominant mode. Please note that in this model the influence of the proportionality coefficients arising from the double integration of Equation (21) over time is overlooked. In reality, both the magnitude and the peak location of the amplitude are affected by this integration. As a result, we expect this model to yield a slight time deviation in predicting the merger position. We assessed the strengths and weaknesses of the BoB model in a previous work [62].

2.3. The Complete Baseline Model

Let us now assemble the two forms of the GW strain by gluing the waveform around the LR at the transition between the weak and strong field, estimated by [54]:

$$r_{LR} = 2M\left[1 + \cos\left(\frac{2}{3}\cos^{-1}(-\chi_f)\right)\right]. \tag{23}$$

Frequency and phase matching is robust against slight variations around this location, while the continuity of the amplitude is best ensured by choosing $r_{LR} \approx 4M$, representing the location of the retrograde photon orbiting a maximally rotating BH.

We stitch the amplitudes of the two models together by first normalizing the BoB amplitude with its peak value and then rescaling the pN amplitude with the normalized BoB amplitude at t_i by using the following formula:

$$\bar{A}_{pN} = A_{pN} \frac{\bar{A}_{BoB}(t_i)}{A_{pN}(t_t)}, \tag{24}$$

where the quantities with an overhead bar represent their rescaled values. We build the complete hybrid model by gluing together the waveforms of the two domains at t_i with the following simple piecewise (step) function:

$$\sigma(t) = \begin{cases} 0 & t < t_i \\ 1 & t \geq t_i \end{cases} \tag{25}$$

For example, the hybrid orbital frequency of the GW has the form:

$$\Omega_{hyb}(t) = (1 - \sigma(t))\Omega_{pN}(t - t_t) + \sigma(t)\Omega_{BoB}(t - t_i), \tag{26}$$

We form the hybrid amplitude, phase, and strain of the GW with the same technique.

Before moving forward, we must test the accuracy of our implementation with a numerical waveform. We chose `SXS:BBH:0180` corresponding to an equal-mass, a non-spinning BBH configuration of normalized mass, and an initial separation of $18M$ in geometric units [44]. We use the same configuration but start our analytic model at a separation of $15M$, which for a regular equal-mass BNS with a total mass of $2.8M$ translates to a distance of about 45km between the centers of mass. We start the BoB model with the initial orbital frequency $(\Omega_i, \dot{\Omega}_i)$ of the pN model at the end of the inspiral marked by the LR and build the hybrid baseline model. Next, we interpolate the NR data onto a time array of constant time steps, as used by the analytical model, to align the strains. We first must decide on an event at which the two waveforms should agree and choose an alignment where the initial frequency of the analytical model matches with the frequency of the numerical data. We then extend this alignment over a window equal to a complete period or GW cycle, between the two initial peaks of the h_+ component of the strain.

In Figure 1, we plot a comparison between the evolution of the h_+ strain component obtained with our hybrid model and the $+$ polarization of the GW strain from the NR simulation, as well as the differences in phase and amplitude (lower insets). We observe a significant overlap between the strain from the analytical model and the NR simulation throughout the entire inspiral, extending up to the LR. The faster merger occurring in the analytical model is primarily attributed to the post-Newtonian (PN) approximation's limited reach into the strong field domain. In subsequent studies, we aim to refine this model by including higher-order post-Newtonian (pN) terms as they become available. The shift in the position of the merger is accentuated by the BoB model because, as we explained earlier, it assumes a simplified expression for the amplitude. We analyzed this deviation from the NR-predicted waveform at the merger in [62], and in future work, we intend to correct the merger amplitude by incorporating the neglected integration coefficients. The phase concordance between the analytical model and the NR data is consistent throughout the entire waveform during the inspiral phase, remaining within the sub-radian accuracy of the BBH numerical waveforms [45]. We see an increase in the phase difference above 1 `rad` only at the LR and reaching 2.8 `rad` by the time of merger, which is within the numerical BNS dephasing due to tidal disruptions [45]. Similarly, the amplitude correlates well up to the LR, with the discrepancy becoming more pronounced as the merger approaches. The addition of tidal effects to this analytic model will overwrite the errors around the merger because a BNS system reaches merger earlier than its corresponding BBH system.

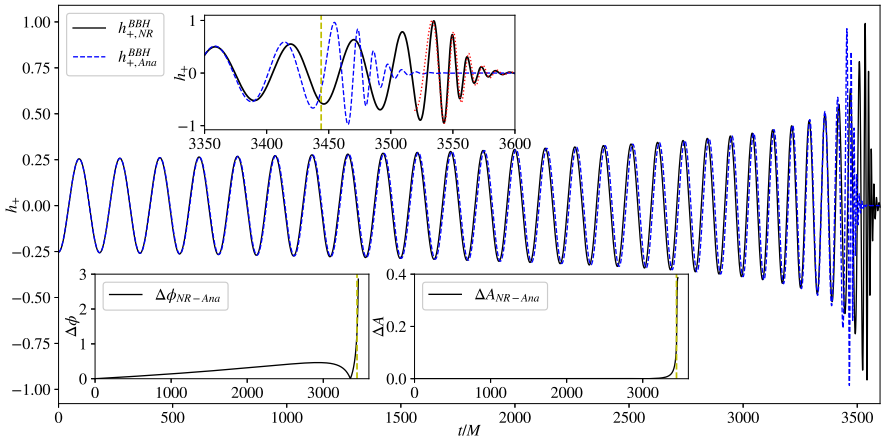

Figure 1. Comparison between the numerical and the analytic h_+ matched over one period around the initial frequency. The upper inset shows that the strain peaks are slightly displaced, but the

merger is well modeled if we overlap them (dotted red curve). The dashed vertical yellow line marks the LR. The two lower insets contain the difference in phase (lower left) and amplitude (lower right) between our model and `SXS:BBH:0180`. Only expected small differences before the merger are visible.

3. Implementation of the Tidal Model

Thus, far, we have not taken into consideration the internal structure of the neutron stars, which is determined by the equation of state and accounts for the effect of the tidal interactions. It is expected for all neutron stars in the universe to be described by a unique equation of state, but its expression is not currently known, only estimated by theory [63] and experiments [64] in nuclear physics. Tidal effects become important in the late stage of the inspiral, inducing deformations in the stars and driving them to merge faster, thus affecting the emitted GW signal both in phase and in amplitude. It is this effect that will allow us to determine the equation of state corresponding to the dense matter inside neutron stars from the direct observations of the amplitude and phase of the gravitational waves emitted during BNS collisions.

We can encode the tidal effects into the tidal correction to the strain:

$$h_T(t) = A_T(t)e^{-2i\phi_T(t)} \tag{27}$$

where A_T and ϕ_T are the analytic tidal corrections to the GW amplitude and phase.

To express the physical influence of tidal effects on the GW amplitude and phase in a manner proportional to the point-particle waveform, we write the BNS strain as follows: $h_{BNS}(t) = h_{BBH}(t) + \delta h_T(t) = h_{BBH}(t)(1 + \delta_T(t)) \approx h_{BBH}(t)h_T(t)$, where $h_{BBH}(t)$ is the point-particle baseline strain, $\delta h_T(t)$ is the additive correction due to tidal effects, and $\delta_T(t)$ is the relative tidal correction factor. We choose to write the $h_T(t)$ factor this way to capture how tidal deformations scale the baseline strain. An equivalent expression is implemented in the LALSuite [39] and given by Equation (9) in [33]. We find the analytical GW strain of the BNS model by multiplying Equation (27) to the strain of the baseline model:

$$h_{BNS}(t) = A_{BNS}(t)e^{-2i\phi_{BNS}(t)} = h_{BBH}(t)h_T(t) = A_{BBH}A_T(t)e^{-2i(\phi_{BBH}(t)+\phi_T(t))}. \tag{28}$$

This equation tells us that we must add the tidal phase correction to the baseline,

$$\phi_{BNS}(t) = \phi_{BBH}(t) + \phi_T(t), \tag{29}$$

while for the amplitude, we should multiply the tidal correction to the baseline:

$$A_{BNS}(t) = A_{BBH}(t)A_T(t). \tag{30}$$

We implement the tidal effects as polynomial functions of the variable $x = (M\Omega_{hyb})^{2/3}$ and build the analytical expressions for the BNS phase and amplitude provided by the pN and NRTidal models, then we validate our implementation by comparing it with two open-source BNS simulations from the SXS catalog [45].

3.1. The BNS Tidal Phase

As the stars become closer together, their tidal deformability increases, affecting the binding orbital energy. Looking back to Equation (1), we should not be surprised to see that this will change the flux of gravitational waves emitted as the orbit shrinks. The tidal correction becomes significant only as the stars approach the merger, not entering in the pN decomposition until the 5th pN correction term [65]. The correction to the GW phase induced by the tidal deformation of one star due to the gravitational pull produced by its companion is known up to 7.5-pN [66], and can be written as follows:

$$\phi_T = \frac{13x^{2.5}}{8\eta}\kappa_{A,eff}\left(1 + c_{A,1}x + c_{A,1.5}x^{1.5} + c_{A,2}x^2 + c_{A,2.5}x^{2.5}\right) + [A \leftrightarrow B] \tag{31}$$

with x from the baseline BBH model and the pN tidal phase coefficients $c_{[A,B],i}$ depending on the mass ratio, as given in [34]. The tidal effects are encoded in $\kappa_{[A,B],eff}$, named the effective tidal coupling constant, introduced in [31]:

$$\kappa_{eff} = \kappa_{A,eff} + \kappa_{B,eff} = \frac{3}{32}(\tilde{\Lambda}_A + \tilde{\Lambda}_B) = \frac{3}{16}\tilde{\Lambda}, \tag{32}$$

where

$$\tilde{\Lambda}_A = \frac{16}{13}\frac{(M_A + 12M_B)M_A^4\Lambda_A}{M^5};\ \ \tilde{\Lambda}_B = \frac{16}{13}\frac{(M_B + 12M_A)M_B^4\Lambda_B}{M^5} \tag{33}$$

are the symmetric mass-weighted tidal deformabilities [28], defined in terms of $\Lambda_{[A,B]}$, the dimensionless tidal deformability of each star in the binary [67]. Let us take a closer look at this quantity, because it is its dependence on the equation of state and mass that can reveal the internal structure of the neutron stars in the binary by measuring the phase of their GW emission and fitting it with analytical or numerical templates. In general, the nuclear models give numerical values for the dimensionless tidal deformability between 10^2 and 10^3, varying inversely proportional with the mass and the compactness of the star [68]. So-called hard nuclear equations of state models describe less compact stars, predicting higher values for the tidal deformability, while nuclear models with soft equations of state favor more compact stars and tidal deformabilities towards lower values. The dimensionless tidal deformability calculated from the GW170817 event gave, for a neutron star of mass $1.4M_\odot$, a value somewhere in the middle range, namely $\tilde{\Lambda} \approx 400$ [69].

We now return to the tidal correction of the GW phase, and, as mentioned before, choose the NRTidal model for supplying the expression of the tidal phase evolution. This analytical approximation, first introduced in [31] and subsequently improved in [33,34], is calibrated to NR, and because of the scarce availability of numerical simulations of BNS systems with unequal mass ratio, includes only non-spinning, equal-mass configurations. However, the model was recently extended to include systems with high-mass ratio systems and a wider range of equations of state in [70].

In this work, we consider the equal-mass case, for which Equation (31) simplifies to a polynomial of constant coefficients:

$$\phi_{T,eq} = \frac{13x^{2.5}}{8\eta}\kappa_{eff}\left(1 + \sum_{i=2}^{N} c_{i/2}x^{i/2}\right) = \frac{13x^{2.5}}{8\eta}\kappa_{eff}P(x). \tag{34}$$

Here, $\phi_{T,eq}$ is the tidal correction to the GW phase for the equal-mass binary. In order to fit Equation (34) to NR data, NRTidal replaces the polynomial $P(x)$ with a rational function $R(x)$ given by a Padé approximant of constant coefficients:

$$R(x) = \frac{1 + n_1x + n_{1.5}x^{1.5} + n_2x^2 + n_{2.5}x^{2.5} + n_3x^3}{1 + d_1x + d_{1.5}x^{1.5} + d_2x^2}, \tag{35}$$

determined from the NR, and restricted to enforce consistency with the analytical coefficients entering the polynomial $P(x)$.

Using one set of coefficients for c_i and two sets of coefficients for (n_i, d_i) from [31,33,34], we implement the tidal correction to our hybrid baseline model as follows:

$$\phi_{T,pN} = \frac{13x^{2.5}}{8\eta}\kappa_{eff}P(x);\ \ \phi_{T,F1(F2)} = \frac{13x^{2.5}}{8\eta}\kappa_{eff}R(x). \tag{36}$$

We denote the pN polynomial approximation to the tidal phase correction as $\phi_{T,pN}$, using the set of coefficients for c_i taken from [31,34]. Next, we indicate the NRTidal fit as $\phi_{T,F1}$ with (n_i, d_i) given in [31,33] and we denote the NRTidalv2 fit as $\phi_{T,F2}$ with

the coefficients (n_i, d_i) given in [34]. Although mass-ratio dependence is included in Equation (36) through the symmetric mass ratio η, the coefficients are derived for equal mass systems. Very recently, the NRTidalv3 fit that extends the model to unequal mass ratio BNS systems was presented in [70]. We will include this model in future work. Note that, in contrast to the corresponding equations presented in [31,33,34], we found it necessary to use a positive sign in Equation (36) in order to obtain the expected behavior for the BNS phase evolution when we use Equation (29) to obtain the analytic BNS phase.

It is time to verify our implementation and test the NRTidal model's ability to predict the tidal phase against numerical simulations. We choose two equal-mass, non-spinning BNS systems with two different equations of state [45], publicly available in the SXS GW catalogue [44]. The first numerical GW used is `SXS:NSNS:0001`, with mass $M_1 = 2.8$ and an ideal gas equation of state of polytropic index $\Gamma = 2$ corresponding to a dimensionless tidal deformability $\tilde{\Lambda}_{\Gamma 2} = 791$. The second is `SXS:NSNS:0002`, with mass $M_2 = 2.7$ and a piecewise polytropic equation of state for cold dense matter called MS1b [71], with a dimensionless tidal deformability $\tilde{\Lambda}_{MS1b} = 1540$. While these tidal deformabilities surpass the one estimated from the GW170817 observation, they are not yet ruled out and are useful as an upper bound. We also note that in the pN and NRTidal models the tidal correction to the phase depends only linearly on the dimensionless tidal deformability, and the coefficients should remain independent of it.

We start with the assumption that at a considerable distance from the merger, the tidal effects are negligible and the BNS signal is virtually indistinguishable from that of the BBH. This allows us to rescale the phase and shift the time of the numerical BNS simulations to start from zero at the reference frequency of each simulation, marking when the initial burst of spurious transient radiation has dissipated in the NR simulation [44]. Then, we find the time and phase corresponding to the same frequency in the numeric BBH model and align the numerical BNS waveforms with the corresponding values of the numeric BBH model over a window of one GW cycle using the same procedure as before. We then calculate the difference in phase between the numeric BNS and BBH data up to the merger frequency, taken where the numeric BNS amplitude reaches its peak.

We plot in Figure 2 the phase comparison between our analytic baseline hybrid model, `SXS:BBH:0180`, `SXS:NSNS:0001` (BNS1), and `SXS:NSNS:0002` (BNS2). The insets in Figure 2 contain the analytical models for the BNS tidal phase $\phi_{T,pN}$ and $\phi_{T,NRfit}$ from Equation (36) compared to the numerical BNS tidal phase. We mark the phase of 2 `rad` with a dashed yellow curve, representing the upper limit of uncertainty in phase due to numeric errors [45]. The maximum modeling error of our baseline BBH phase in the domain considered is below 0.5 `rad`. We observe that the NRTidal phase (dash-dot-dot red and magenta) slightly overestimates both the pN (dotted maroon) and the NR phase and is more accurate for the BNS1 case, corresponding to the smaller tidal deformabiliy. This suggests that the assumption of the coefficients being independent of the tidal deformability may be too restrictive. In Section 4, we will delve into the behavior of the phase around the merger and propose new coefficients for the tidal correction to push the model past the merger.

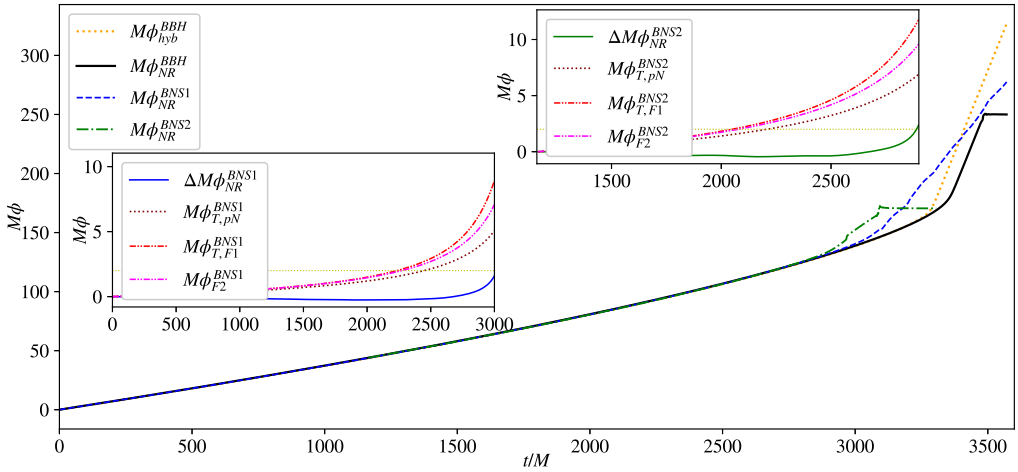

Figure 2. Phase comparison between the baseline model (solid orange), `SXS:BBH:0180` (solid black), `SXS:NSNS:0001` (dashed blue), and `SXS:NSNS:0002` (dash-dot green) overlapped at the reference frequencies of the NR simulations. The insets contain our analytical BNS phase calculated with the pN (dotted maroon) and NRTidal (dash-dot-dot red and magenta) corrections, plotted up to the merger against the numerical phase difference for the two cases. The horizontal dotted yellow curve marks the maximum uncertainty in phase of 2 `rad`.

3.2. The BNS Tidal Amplitude

The amplitude of the GW is extremely small, and its increase is less dramatic than the phase accumulation observed up to the merger, defined as the point of maximum amplitude [72]. This makes the task of accurately modeling analytic tidal contributions to the amplitude more difficult compared to the phase. Taking advantage of the relatively small change in the GW amplitude, we can effectively use a low-order polynomial within the context of the pN approximation of the form [34,66]:

$$A_T(x) = \frac{8M\eta}{D_L}\sqrt{\frac{\pi}{5}}x^6\kappa_{eff,A}(\hat{c}_{A,0} + \hat{c}_{A,1}x) + [A \leftrightarrow B], \tag{37}$$

where D_L is the distance from the detector to the BNS system and $\hat{c}_{[A,B],i}$ are the pN tidal amplitude coefficients, given in [34,66]. Let us assume again a similar-mass binary, where only the symmetric mass ratio η retains the information on the mass ratio. Now, the pN tidal correction in amplitude Equation (37) simplifies to the following:

$$A_{T,pN}(x) = A_{T,eq}(x) = \frac{M\eta}{21D_L}\sqrt{\frac{\pi}{5}}x^6\kappa_{eff}(672 - 11x). \tag{38}$$

As expected, this approximation becomes less reliable as the binary approaches the merger. The NRTidal model corrects it by adding a dependence of x:

$$A_{T,d}(x) = \frac{A_{T,pN}(x)}{1 + dx}, \tag{39}$$

where the parameter d is fixed by the identity [34]:

$$d = \frac{1}{x}\left(\frac{A_{T,pN}(x)}{A_{mrg}} - 1\right)\Big|_{x=x_{mrg}}. \tag{40}$$

We compute the merger amplitude A_{mrg} using an analytically predicted quasi-universal relation valid at the moment of merger [73], that provides the peak amplitude only as a function of the tidal coupling constant κ_{eff} [34]:

$$A_{mrg} = \frac{M\eta}{D_L} \frac{1.6498(1 + 2.5603 \times 10^{-2}\kappa_{eff} - 1.024 \times 10^{-5}\kappa_{eff}^2)}{1 + 4.7278 \times 10^{-2}\kappa_{eff}}. \tag{41}$$

As a cautionary remark, Equation (40) requires that we provide an analytical expression for x_{mrg} as well, without relying on numerical data. A good approximation is to assume that the stars merge when they come in contact, and x_{mrg} is given by the following:

$$x_c = \frac{M}{R_A + R_B}, \tag{42}$$

where $R_{A,B}$ are the radii of the stars, for which we use the value of 11.5km as specified in [45]. Please note that this simplified expression does not account for the deformations in the stars. To address this, we use an alternative route and calculate $x_{mrg} = (M\Omega_{mrg})^{2/3}$ from the analytic expression for the merger frequency given in [74]:

$$M\Omega_{mrg} = \sqrt{q} \frac{0.178(1 + 3.354 \times 10^{-2}\kappa_{eff} + 4.315 \times 10^{-5}\kappa_{eff}^2)}{1 + 7.542 \times 10^{-2}\kappa_{eff} + 2.236 \times 10^{-4}\kappa_{eff}^2)}. \tag{43}$$

We chose to use the result calculated with Equation (43) in our implementation. Working within the same assumption that the BNS and BBH waveforms have indistinguishable amplitudes far from the merger, we rescale the numeric BNS amplitude to coincide with the numeric BBH amplitude for a binary with the same total mass at the reference frequency. We align the BNS and BBH amplitudes and plot them in Figure 3. This is not fulfilled exactly, as we see in the inset of Figure 3, where we plot a comparison of their h_+ strain because at the BNS reference frequency tidal effects are already present in the NR waveforms.

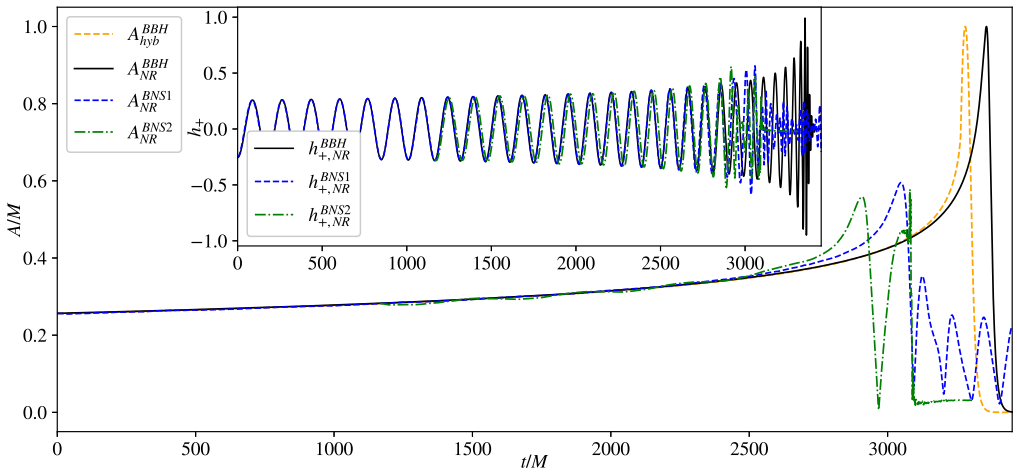

Figure 3. Amplitude comparison between SXS:NSNS:0001 (dashed blue) and SXS:NSNS:0002 (dash-dot green) rescaled at the reference frequencies of the NR simulations. The inset contain a comparison of the numerical h_+ between the BNS and BBH data.

Let us now add the tidal amplitude correction to our baseline model, using Equation (30). We assume that the amplitudes are indistinguishable at the reference frequency of the numerical BNS data, although the waveform is already in the regime where tidal effects are non-negligible. Nonetheless, we assume that this error in amplitude is not essential for

our analysis and consider that $A_{T,ref} \approx 1$. We capture this behavior for the evolution of our analytic BNS amplitude by changing A_T to the following:

$$A_T(x) \to 1 + A_T(x). \tag{44}$$

In Figure 4, we plot the ratio of the amplitudes for BNS1 (`SXS:NSNS:0001`) and BNS2 (`SXS:NSNS:0002`) to the amplitude of the numeric BBH (`SXS:BBH:0180`) compared with the ratio of our hybrid analytic baseline amplitude to the numeric BBH amplitude. The insets in Figure 4 contain the analytical approximations for the BNS tidal amplitude, as in Equations (38) and (39), up to the corresponding BNS merger frequency. We observe that both analytical approximations underestimate the steep increase in amplitude around the merger. We will return to this comparison in Section 4, when we will make a new fit for the analytical amplitude to the numerical data and taper the amplitude past the merger using a Hann window.

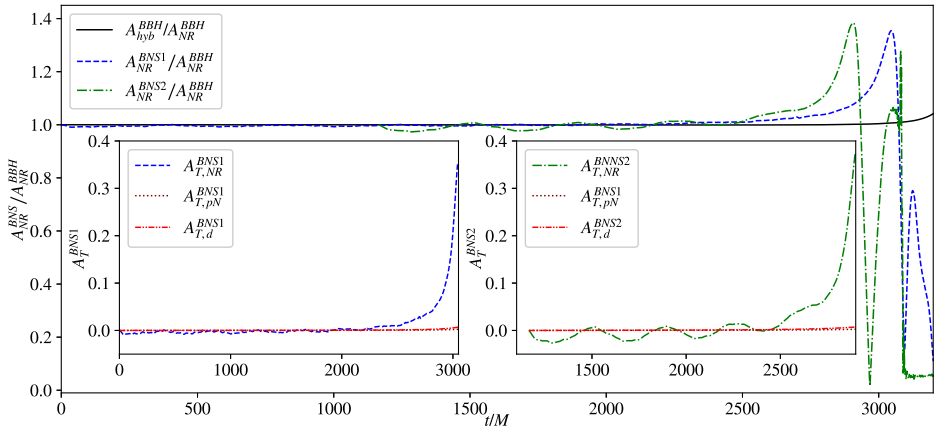

Figure 4. Amplitude comparison between the baseline model (solid black), `SXS:NSNS:0001` (dashed blue) and `SXS:NSNS:0002` (dash-dot green) overlapped at the reference frequencies of the NR simulations and divided by the amplitude for SXS:BBH:0180. The insets contain (**left**) the amplitudes for the tidal pN (dotted maroon) approximation and (**right**) for the NRTidal (dash-dot-dot red) approximation, plotted up to the merger against the numerical BNS amplitude for the two cases.

4. Modeling the BNS Merger

Up to this point, we presented the analytical formulas we implemented in our code RisingTides to model the tidal effects on GWs from BNS systems up to the merger. Our tests confirmed that both the pN and NRTidal approximations hold reasonably well in comparison with the two numerical relativity simulations considered, although they were not included in the original calibrations [31,33,34]. Let us now take a closer look at the behavior of the analytical models for the tidal phase and amplitude as we approach the merger. Indeed, we shall see a heightening of the mismatch with the numerical simulations and will attempt to improve the model by performing our own fit only up to the merger. Because of the smooth evolution of the phase and amplitude even after the moment of the merger, we can use the new coefficients obtained from our fit to push the model past the location where the stars touch. We extend the model for the phase beyond the merger and devise a method to determine how far we can reach, where we end it with a taper and continue with the baseline model. We carry the amplitude up to the merger and terminate it with a Hann taper to ensure a smooth and continuous transition into the post merger.

4.1. New Fit for the Tidal Phase

Let us proceed by first taking the difference between the numerical BNS and BBH phase for the two systems considered. This is the *true* tidal correction (up to $\pm$`2rad`. numerical error [45]) that we subsequently use to compare with the analytical models for the tidal phase. We plot in the left side of Figure 5 the difference between the numerical

tidal phase and the three analytical approximations for $\phi_{T,pN}$, $\phi_{T,F1}$, and $\phi_{T,F2}$ with the coefficients from [31,33,34]. We start at a time about $1000M$ before the merger, where the differences between the analytic and numerical phase become noticeable. We then extend the model past the merger, until the approximation exhibits a sharp increase and breaks down. We observe an increased difference between the analytical and numerical tidal phase near the merger, above the uncertainty of $\pm 2\mathrm{rad}$. In the right side of Figure 5 we plot the true tidal phase (upper plot), as well as the scaled tidal deformability (lower plot). The true tidal phase scales with the tidal deformability before the merger, as expected, but after the merger is larger for the first (BNS1) system compared to the second (BNS2), appearing to scale inversely with the tidal deformability. The analytical phase, which depends linearly on the tidal deformability, does not provide an accurate estimation after the merger. Specifically, the post-merger tidal phase is underestimated for the first system and overestimated for the second.

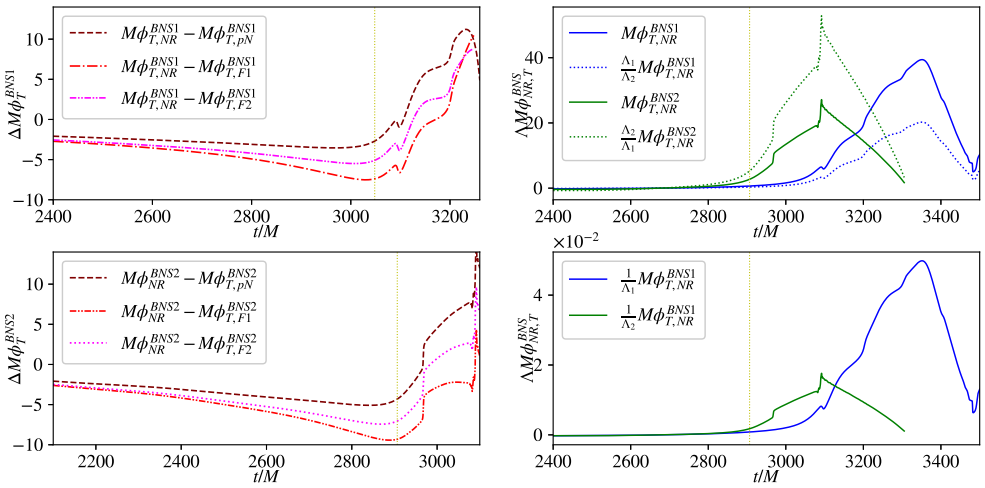

Figure 5. Left plots: Difference between the numerical tidal phase correction and the analytic pN and the three NRTidal models (pN, *F*1 and *F*2) for the tidal phase applied to the two BNS systems close to the merger and extended beyond it. Right plots: true and rescaled tidal phases for the two BNS systems, overlapped at the merger time. The vertical yellow dotted line marks the merger.

We assume that the Padé approximant from Equation (35) is complex enough to model the smooth increase in the tidal phase at the merger and proceed with performing new curve fits for the analytical tidal phase to the numerical tidal phase scaled by the tidal deformability. As initial guesses, we use the coefficients from the pN [31], *F*1 [33] and *F*2 [34] NRTidal model and stop the fit at the merger. Irrespective of the initial fitting coefficients, we obtain comparable sets of new coefficients for the polynomial modeling the tidal interaction of a BNS system with a given deformability. However, in contrast to the original fits, we no longer find a one-size-fits-all set of coefficients, namely, our coefficients depend on the equation of state considered.

To select the best fit among the three variations of the analytical model, we calculate and compare the sum of squared residuals (SSR) for each numerical dataset. For BNS1, we select new parameters obtained by fitting to the numerical data, using the *F*2 coefficients as the initial guess. For BNS2, we choose the parameters derived from fitting the numerical data with the *F*1 coefficients as initial guess. Subsequently, we compare the residuals for the chosen coefficients between the two datasets and select the optimal fitting parameters for BNS1 as the new coefficients.

In Table 1, we provide the average values of the new coefficients obtained for BNS1 in comparison with the *F*2 NRTidal coefficients.

We need to alert readers that the large differences between our new fitting coefficients and the original ones are primarily due to our efforts to model the highly nonlinear tidal interactions during the merger, which is a step beyond the bounds of the analytical approximation. The assumptions made in the original model that the coefficients were independent of the equation of state are no longer applicable.

We use the new fitting coefficients to reconstruct the analytical tidal phase, then we incorporate it into the baseline framework, thus obtaining a new analytical model for the BNS phase that extends beyond the merger. Following this, we develop a procedure that determines the termination point of our phase, where we apply a Heaviside function, allowing only the phase of the baseline model to continue from then on. First, we calculate the difference between our new analytical tidal phase and the true tidal phase. After that, we determine the time derivative of this difference. Next, we identify potential cutoff points at locations where this derivative switches sign. Lastly, we select the final cutoff point as the last point for which the deviation from the numerical phase is less than 3%, to optimize the fit with the true tidal phase. Here we terminate our analytical tidal phase with a Heaviside function and continue smoothly with the baseline phase, obtaining a complete phase representation.

In Figure 6, we plot our newly modeled phase. In the main plot, we show our new analytic fit for the BNS phase tailored to the two BNS systems against the true tidal phase. Although we applied the curve fit only up to the merger, we see that it is able to accurately follow the numerical tidal phase beyond the merger. In the two insets, we include a comparison between our reassembled tidal phase for the two BNS systems with the Heaviside taper applied at the cutoff point and the numerical BNS phase. We test our new model for BNS1 against the NR data for BNS2 and include the new fit in the second inset (dash-dot-dot light green). We see that our model is accurate up to the moment of the merger, but it underestimates the steep increase in phase in the early post-merger, which is motivated by our findings that in the post-merger the phase does not scale linearly with the tidal deformability.

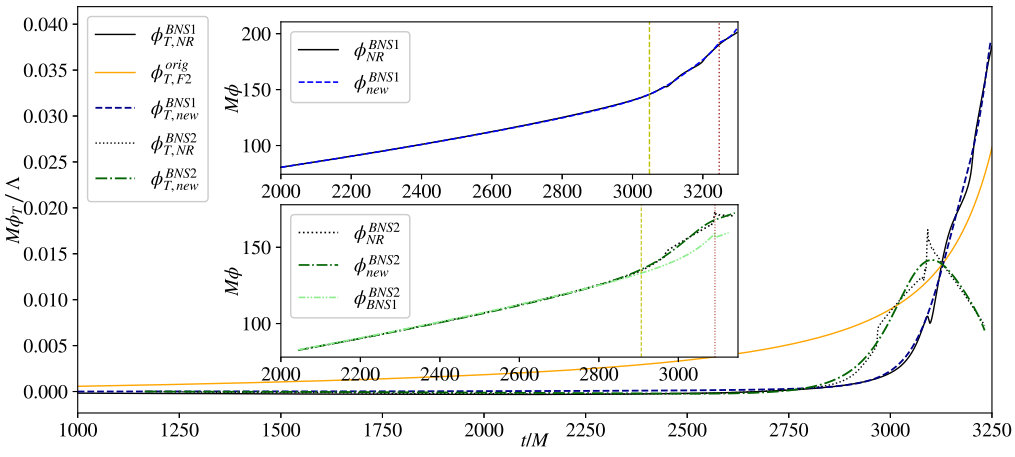

Figure 6. Comparison between our analytic new fit to the tidal phase (dashed blue and dash-dot green) to the numerical tidal phase (solid and dotted black), as well as the original *F*2 fit (solid orange) for the two BNS systems up to the merger then continued beyond the merger. The insets contain the reconstructed BNS phase for the two BNS systems extended beyond the merger as well as the new fit with the chosen coefficients for BNS1 to BNS2 (dash-dot-dot light green). The vertical yellow dotted line marks the merger, and the vertical brown dotted line delineates the end point where tapered.

Table 1. New merger fit for tidal phase dependent on the tidal deformability.

Coefficient	Original $F2$ Fit [1]	New Fit
n_1	−15.2452	−214.95
$n_{1.5}$	31.5423	2016.23
n_2	−80.9260	−7743.40
$n_{2.5}$	312.482	13,772.45
n_3	−342.155	−9381.96
d_1	−20.2372	−42.62
$d_{1.5}$	39.3962	151.06
d_2	−5.36163	−150.08

[1] as given in [34].

4.2. New Fit for the Tidal Amplitude

We use a similar procedure to model the analytical amplitude at the merger and start by calculating the numerical tidal amplitude as the ratio between the numerical BNS and BBH amplitudes for the two systems considered. This is the true tidal amplitude that we use next to compare with the analytical approximations $A_{T,pN}$ and $A_{T,d}$. We attempt to improve the amplitude modeling by applying a curve fit for Equations (38) and (39) to the true tidal amplitude up to the merger, using the coefficients given in [34] as the initial guesses. Again, we obtain similar sets of new coefficients regardless of the model we start with but depending on the value of the tidal deformability. We apply again the same procedure of calculating and comparing the sum of squared residuals (SSR) and select the optimal fitting parameters for BNS1 amplitude as the new coefficients.

In Table 2, we give the values of the new coefficients resulting from the new tidal amplitude fit in comparison with the $A_{T,d}$ NRTidal coefficients.

Table 2. New merger fit for tidal amplitude dependent on the tidal deformability.

Coefficient	Original $A_{T,d}$ Fit [1]	New Fit
d	−5.96	−1.3176
p	1	0.1318

[1] as given in [34].

With these coefficients, we proceed to reconstruct the new analytical amplitude. This time, we cannot track the amplitude beyond the merger due to its unphysical steep increase. While the model is precise enough to capture the sharp rise in amplitude before the merger, it is too basic to accurately follow its evolution beyond the peak point. To complete the waveform beyond the merger, we taper the amplitude at the merger with a Hann window that terminates to zero at the phase cutoff time.

In Figure 7, we plot a comparison between the numerical BNS amplitude and our new amplitude with tides. The two insets display our fit to the numerical tidal amplitude, contrasted with the pN and NRTidal tidal amplitudes for the two BNS systems. We again apply our new model for BNS1 to BNS2 and test it against the NR data for BNS2, including the new fit in the second inset (dash-dot-dot light green), and observe an improvement comparing to the original fit.

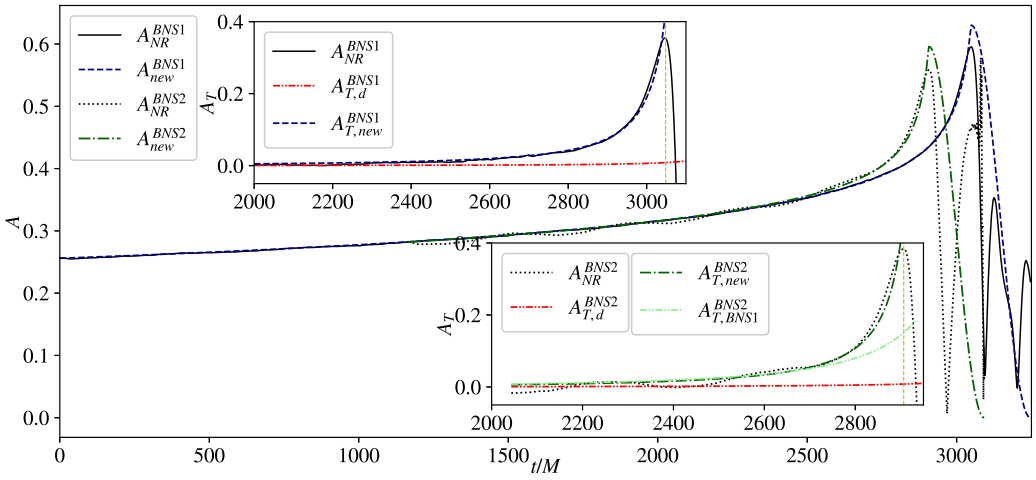

Figure 7. Comparison between the two numerical BNS amplitudes (solid and dotted black) and our new fit for the amplitudes (dashed blue and dash-dot green) up to the merger, then tapered by a Hann function between merger and the cutoff time for the phase. The insets include our fit to the numerical tidal amplitude compared with $A_{T,d}$ as well as the new fit with the chosen coefficients for BNS1 to BNS2 (dash-dot-dot light green). The vertical yellow dotted line marks the merger.

4.3. A Toy Model for the Complete Analytic BNS Waveforms

With these new fits obtained for the phase and amplitude, we build a complete analytical GW strain for the BNS merger using Equation (28). Although we overlooked the amplitude complexity after the merger, we modeled the phase accurately up to the cutoff time. This allows us to recompute the orbital frequency Ω_{BNS} by taking the time derivative of the phase ϕ_{BNS}. Then, we recalculate x_{BNS} and follow with the radial separation r_{BNS}, using Equation (5). We also reevaluate the orbital and radial velocities and compare their evolution through the merger. Looking at their ratio we observe that even at the merger, where the radial velocity reaches its maximum, it represents at most 6% of the orbital velocity, after which it falls abruptly. In contrast, the orbital velocity keeps increasing even after the merger, reaching its peak soon thereafter, after which it starts decreasing as well. The domain between merger and cutoff time is very short, extending only up to $240M$ for BNS1 and $180M$ for BNS2. For the systems considered, this is between 2 ms and 3 ms, not enough to inform us on the fate of the remnant. Most likely, we reach the early stages of a rapidly rotating, tidally deformed remnant. The GW170817 event indicates that a remnant with a total mass of $2.8M_\odot$ will settle as a neutron star, with the collapse to a black hole being less likely [4].

Note that our toy model does not account for the mass ejected due to the tidal interactions during coalescence or the dynamically ejected mass during the collision-induced shock of the neutron star crust when the stars come in contact. The matter expulsion at the contact interface is called shock ejecta and represents a significant source of ejecta for systems with similar masses to those considered in this work. Additionally, our model excludes the neutrino-driven wind ejecta emitted by the HMNS remnant as it cools down. The different types of ejecta produced during the BNS evolution form a rotating disk surrounding the remnant. The total mass ejected by the GW170817 event was estimated to be about $0.04M_\odot$, and this is the value we consider in our work.

In Figure 8, we plot the h_+ component of the strain for the baseline model in comparison with the BNS strain for the two equations of state considered. While our model for the amplitude past the merger is simplified, the phase modeling remains accurate. In the left plot of Figure 8, we show the evolution of the separation between the neutron stars for the two equations of state considered continued beyond the merger, depicted with the red dotted circle, in comparison to the separation of the baseline BBH model. We see how the value of the tidal deformability and thus of the equation of state influence the early stages

before and beyond the collision, revealing the effect of the matter interaction on the orbits. A larger tidal deformability (dashdot cyan) speeds up the merger of the stars, leading to a larger-radius remnant, whereas a smaller value for it (dotted blue) prolongs the inspiral and yields a denser remnant with a smaller radius.

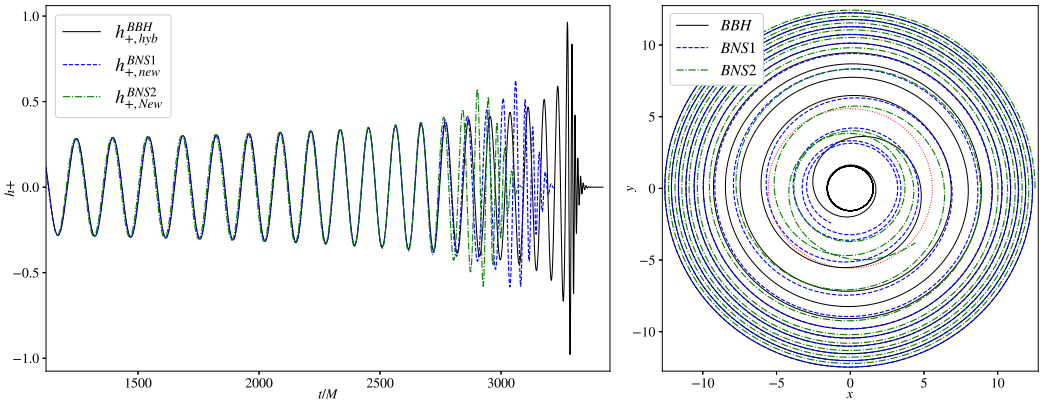

Figure 8. Our analytical strain (left plot) and separation (right plot) for the baseline BBH (solid black), the $\Lambda = 791$ BNS1 (dotted blue) and the $\Lambda = 1520$ BNS2 (dashdot cyan) for the last $\approx$10 orbits extended to the early stages of the collision. The dotted red line marks where the neutron stars touch.

5. Discussion

The gravitational waves emitted during a BNS merger offer insights into the behavior of matter under extreme conditions. To understand the impact of matter on the evolution of such systems and on their gravitational waves signature, we embarked upon an analytical modeling journey. Initially, we focused on a BBH system, employing the post-Newtonian formalism for the inspiral and the Backwards-one-Body model for the merger. By combining them, we established a baseline waveform, which we validated against numerical relativity simulations to ensure a robust foundation for our next step. To incorporate the effects of tides, we introduced corrections to the phase and amplitude of the point-particle waveform by using the polynomial expressions proposed by the NRTidal model. We then verified the model's accuracy and efficiency through careful comparison with numerical relativity data for two equations of state.

However, we encountered a mismatch around the merger when solely relying on the NRTidal model. To address this limitation, we lifted the restriction on the coefficients' independence from tidal deformability and recalibrated them with the numerical relativity predictions. By performing new fits to the numerical BNS data, we obtained updated values for the polynomial coefficients. Armed with these new coefficients, we reconstructed the tidal corrections and achieved improved fits for the phase and amplitude, successfully extending the phase modeling beyond the merger. To achieve a comprehensive phase representation, we devised a method to determine its extent and applied a taper at the end, seamlessly continuing with the baseline model. Regarding the amplitude modeling, we have successfully carried it up to the merger, where we employed a Hann taper to ensure a smooth and continuous transition into the post-merger. We ended by reconstructing the complete analytical BNS strain and by investigating the tidal influence on the system's orbits around the BNS collision.

We developed RisingTides, a Python code guided by a user-friendly Jupyter Notebook for the analytical modeling the tidal effects on the gravitational waves emitted during BNS inspiral and merger. We make our implementation available to the scientific community to foster learning and facilitate further investigations.

In our future work, we aim to enhance our model by incorporating a broader range of numerical relativity BNS simulations encompassing diverse equations of state. We will seek to uncover a consistent pattern for the dependence of the phase on the tidal deformability around the merger, ultimately leading to a universal set of polynomial

coefficients. Furthermore, we will explore universal relations for BNS systems, which may offer deeper insights into their behavior and characteristics. Additionally, we are committed to refining the accuracy of the amplitude modeling beyond the merger, thus increasing the overall predictive power of our approach. Our research will contribute to a better understanding of BNS mergers and their gravitational wave signatures.

Author Contributions: M.C.B.H. initiated and led the project, led the writing and editing of the manuscript, analyzed the data, and produced the figures. A.O. led the code development and contributed to the data analysis. Both authors listed significantly contributed directly and intellectually to this work and give their approval for its publication. All authors have read and agreed to the published version of the manuscript.

Funding: This research was supported in part by the National Science Foundation under Grant No. NSF PHY-1748958.

Data Availability Statement: The datasets generated and analyzed during the current study are openly available at https://github.com/mbabiuc/RisingTides.git (accessed on 20 June 2024), linked to the open-access `Zenodo` repository, at https://zenodo.org/badge/latestdoi/671997364 (accessed on 20 June 2024).

Acknowledgments: The authors are wishing to acknowledge the Physics Department and the College of Science at Marshall University.

Conflicts of Interest: The authors declare no conflict of interest. The funders had no role in the design of the study; in the collection, analyses, or interpretation of data; in the writing of the manuscript; or in the decision to publish the results.

Abbreviations

The following abbreviations are used in this manuscript:

GW	Gravitational Wave
BNS	Binary Neutron Star
BBH	Binary Black Hole
pN	post-Newtonian
EOB	Effective-One-Body
NR	numerical relativity
BoB	Backwards-one-Body
SXS	Simulating eXtreme Spacetimes
ISCO	innermost stable circular orbit
LR	light-ring

References

1. Abbott, B.P.; Abbott, R.; Abbott, T.; Acernese, F.; Ackley, K.; Adams, C.; Adams, T.; Addesso, P.; Adhikari, R.X.; Adya, V.B.; et al. GW170817: Observation of Gravitational Waves from a Binary Neutron Star Inspiral. *Phys. Rev. Lett.* **2017**, *119*, 161101. [CrossRef] [PubMed]
2. Abbott, B.P.; Abbott, R.; Abbott, T.D.; Acernese, F.; Ackley, K.; Adams, C.; Adams, T.; Addesso, P.; Adhikari, R.X.; Adya, V.B.; et al. Gravitational Waves and Gamma-Rays from a Binary Neutron Star Merger: GW170817 and GRB170817A. *Astrophys. J. Lett.* **2017**, *848*, L13. [CrossRef]
3. Arcavi, I.; Hosseinzadeh, G.; Howell, D.A.; McCully, C.; Poznanski, D.; Kasen, D.; Barnes, J.; Zaltzman, M.; Vasylyev, S.; Maoz, D.; et al. Optical emission from a kilonova following a gravitational-wave-detected neutron-star merger. *Nature* **2017**, *551*, 64–66. [CrossRef]
4. Abbott, B.P.; Abbott, R.; Abbott, T.D.; Acernese, F.; Ackley, K.; Adams, C.; Adams, T.; Addesso, P.; Adhikari, R.X.; Adya, V.B.; et al. GW170817: Measurements of Neutron Star Radii and Equation of State. *Phys. Rev. Lett.* **2019**, *121*, 161101. [CrossRef] [PubMed]
5. Malik, T.; Alam, N.; Fortin, M.; Providência, C.; Agrawal, B.K.; Jha, T.K.; Kumar, B.; Patra, S.K. GW170817: Constraining the nuclear matter equation of state from the neutron star tidal deformability. *Phys. Rev. C* **2018**, *98*, 035804. [CrossRef]
6. Bhat, S.A.; Bandyopadhyay, D. Neutron star equation of state and GW170817. *J. Phys. G Nucl. Part. Phys.* **2019**, *46*, 014003. [CrossRef]
7. Abdalla, H.; Adam, R.; Aharonian, F.; Benkhali, F.A.; Angüner, E.O.; Arakawa, M.; Arcaro, C.; Armand, C.; Armstrong, T.; Ashkar, H.; et al. Probing the Magnetic Field in the GW170817 Outflow Using H.E.S.S. Observations. *Astrophys. J. Lett.* **2020**, *894*, 16. [CrossRef]

8. Wu, Y.; MacFadyen, A. Constraining the Outflow Structure of the Binary Neutron Star Merger Event GW170817/GRB170817A with a Markov Chain Monte Carlo Analysis. *Astrophys. J.* **2018**, *869*, 55. [CrossRef]
9. Nitz, A.H.; Capano, C.D.; Kumar, S.; Wang, Y.F.; Kastha, S.; Schäfer, M.; Dhurkunde, R.; Cabero, M. 3-OGC: Catalog of Gravitational Waves from Compact-binary Mergers. *Astrophys. J.* **2021**, *922*, 76. [CrossRef]
10. Abbott, B.P.; Abbott, R.; Abbott, T.D.; Abraham, S.; Acernese, F.; Ackley, K.; Adams, C.; Adhikari, R.X.; Adya, V.B.; Affeldt, C.; et al. GW190425: Observation of a Compact Binary Coalescence with Total Mass $\sim 3.4\,M_{\odot}$. *Astrophys. J. Lett.* **2020**, *892*, L3. [CrossRef]
11. Safarzadeh, M.; Ramirez-Ruiz, E.; Berger, E. Does GW190425 Require an Alternative Formation Pathway than a Fast-merging Channel? *Astrophys. J.* **2020**, *900*, 13. [CrossRef]
12. Ciolfi, R. Binary neutron star mergers after GW170817. *Front. Astron. Space Sci.* **2020**, *7*, 27. [CrossRef]
13. Lazzati, D.; Perna, R.; Ciolfi, R.; Giacomazzo, B.; López-Cámara, D.; Morsony, B. Two Steps Forward and One Step Sideways: The Propagation of Relativistic Jets in Realistic Binary Neutron Star Merger Ejecta. *Astrophys. J. Lett.* **2021**, *918*, L6. [CrossRef]
14. Hall, E.D.; Evans, M. Metrics for next-generation gravitational-wave detectors. *Class. Quantum Gravity* **2019**, *36*, 225002. [CrossRef]
15. Reitze, D.; Adhikari, R.X.; Ballmer, S.; Barish, B.; Barsotti, L.; Billingsley, G.; Brown, D.A.; Chen, Y.; Coyne, D.; Eisenstein, R.; et al. Cosmic Explorer: The U.S. Contribution to Gravitational-Wave Astronomy beyond LIGO. *Bull. Am. Astron. Soc.* **2019**, *51*, 035.
16. Maggiore, M.; Van Den Broeck, C.; Bartolo, N.; Belgacem, E.; Bertacca, D.; Bizouard, M.A.; Branchesi, M.; Clesse, S.; Foffa, S.; García-Bellido, J.; et al. Science Case for the Einstein Telescope. *J. Cosmol. Astropart. Phys.* **2020**, *03*, 050. [CrossRef]
17. Barausse, E.; Berti, E.; Hertog, T.; Hughes, S.A.; Jetzer, P.; Pani, P.; Sotiriou, T.P.; Tamanini, N.; Witek, H.; Yagi, K.; et al. Prospects for Fundamental Physics with LISA. *Gen. Rel. Grav.* **2020**, *52*, 81. [CrossRef]
18. Kawamura, S.; Ando, M.; Seto, N.; Sato, S.; Musha, M.; Kawano, I.; Yokoyama, J.I.; Tanaka, T.; Ioka, K.; Akutsu, T.; et al. Current status of space gravitational wave antenna DECIGO and B-DECIGO. *Prog. Theor. Exp. Phys.* **2021**, *2021*, 05A105. [CrossRef]
19. Luo, J.; Chen, L.S.; Duan, H.Z.; Gong, Y.G.; Hu, S.; Ji, J.; Liu, Q.; Mei, J.; Milyukov, V.; Sazhin, M.; et al. TianQin: A space-borne gravitational wave detector. *Class. Quantum Gravity* **2016**, *33*, 035010. [CrossRef]
20. Vines, J.E.; Flanagan, E.E. First-post-Newtonian quadrupole tidal interactions in binary systems. *Phys. Rev. D* **2013**, *88*, 024046. [CrossRef]
21. Bernuzzi, S.; Nagar, A.; Thierfelder, M.; Brügmann, B. Tidal effects in binary neutron star coalescence. *Phys. Rev. D* **2012**, *86*, 044030. [CrossRef]
22. Bernuzzi, S.; Nagar, A.; Dietrich, T.; Damour, T. Modeling the Dynamics of Tidally Interacting Binary Neutron Stars up to the Merger. *Phys. Rev. Lett.* **2015**, *114*, 161103. [CrossRef] [PubMed]
23. Akcay, S.; Bernuzzi, S.; Messina, F.; Nagar, A.; Ortiz, N.; Rettegno, P. Effective-one-body multipolar waveform for tidally interacting binary neutron stars up to merger. *Phys. Rev. D* **2019**, *99*, 044051. [CrossRef]
24. Buonanno, A.; Damour, T. Effective one-body approach to general relativistic two-body dynamics. *Phys. Rev. D* **1999**, *59*, 084006. [CrossRef]
25. Damour, T.; Nagar, A. Effective one body description of tidal effects in inspiralling compact binaries. *Phys. Rev. D* **2009**, *81*, 084016. [CrossRef]
26. Hinderer, T.; Taracchini, A.; Foucart, F.; Buonanno, A.; Steinhoff, J.; Duez, M.; Kidder, L.E.; Pfeiffer, H.P.; Scheel, M.A.; Szilagyi, B.; et al. Effects of Neutron-Star Dynamic Tides on Gravitational Waveforms within the Effective-One-Body Approach. *Phys. Rev. Lett.* **2016**, *116*, 181101. [CrossRef] [PubMed]
27. Nagar, A.; Bernuzzi, S.; Del Pozzo, W.; Riemenschneider, G.; Akcay, S.; Carullo, G.; Fleig, P.; Babak, S.; Tsang, K.W.; Colleoni, M.; et al. Time-domain effective-one-body gravitational waveforms for coalescing compact binaries with nonprecessing spins, tides, and self-spin effects. *Phys. Rev. D* **2018**, *98*, 104052. [CrossRef]
28. Favata, M. Systematic Parameter Errors in Inspiraling Neutron Star Binaries. *Phys. Rev. Lett.* **2014**, *112*, 101101. [CrossRef]
29. Dietrich, T.; Hinderer, T. Comprehensive comparison of numerical relativity and effective-one-body results to inform improvements in waveform models for binary neutron star systems. *Phys. Rev. D* **2017**, *95*, 124006. [CrossRef]
30. Gamba, R.; Breschi, M.; Bernuzzi, S.; Agathos, M.; Nagar, A. Waveform systematics in the gravitational-wave inference of tidal parameters and equation of state from binary neutron-star signals. *Phys. Rev. D* **2021**, *103*, 124015. [CrossRef]
31. Dietrich, T.; Bernuzzi, S.; Tichy, W. Closed-form tidal approximants for binary neutron star gravitational waveforms constructed from high-resolution numerical relativity simulations. *Phys. Rev. D* **2017**, *96*, 121501. [CrossRef]
32. Kawaguchi, K.; Kiuchi, K.; Kyutoku, K.; Sekiguchi, Y.; Shibata, M.; Taniguchi, K. Frequency-domain gravitational waveform models for inspiraling binary neutron stars. *Phys. Rev. D* **2018**, *97*, 044044. [CrossRef]
33. Dietrich, T.; Khan, S.; Dudi, R.; Kapadia, S.J.; Kumar, P.; Nagar, A.; Ohme, F.; Pannarale, F.; Samajdar, A.; Bernuzzi, S.; et al. Matter imprints in waveform models for neutron star binaries: Tidal and self-spin effects. *Phys. Rev. D* **2019**, *99*, 024029. [CrossRef]
34. Dietrich, T.; Samajdar, A.; Khan, S.; Johnson-McDaniel, N.K.; Dudi, R.; Tichy, W. Improving the NRTidal model for binary neutron star systems. *Phys. Rev. D* **2019**, *100*, 044003. [CrossRef]
35. Narikawa, T.; Uchikata, N.; Kawaguchi, K.; Kiuchi, K.; Kyutoku, K.; Shibata, M.; Tagoshi, H. Reanalysis of the binary neutron star mergers GW170817 and GW190425 using numerical-relativity calibrated waveform models. *Phys. Rev. Res.* **2020**, *2*, 043039. [CrossRef]
36. Narikawa, T.; Uchikata, N. Follow-up analyses of the binary-neutron-star signals GW170817 and GW190425 by using post-Newtonian waveform models. *Phys. Rev. D* **2022**, *106*, 103006. [CrossRef]

37. Abbott, R.; Abbott, T.D.; Acernese, F.; Ackley, K.; Adams, C.; Adhikari, N.; Adhikari, R.X.; Adya, V.B.; Affeldt, C.; Agarwal, D.; et al. GWTC-2.1: Deep Extended Catalog of Compact Binary Coalescences Observed by LIGO and Virgo During the First Half of the Third Observing Run. *Phys. Rev. D* **2024**, *109*, 022001. [CrossRef]
38. Puecher, A.; Dietrich, T.; Tsang, K.W.; Kalaghatgi, C.; Roy, S.; Setyawati, Y.; Van Den Broeck, C. Unraveling information about supranuclear-dense matter from the complete binary neutron star coalescence process using future gravitational-wave detector networks. *Phys. Rev. D* **2023**, *107*, 124009. [CrossRef]
39. LIGO Scientific Collaboration. LALSuite: LIGO Scientific Collaboration Algorithm Library Suite. 2020. Available online: https://ui.adsabs.harvard.edu/abs/2020ascl.soft12021L/abstract (accessed on 20 June 2024)
40. Buskirk, D.; Babiuc Hamilton, M.C. A complete analytic gravitational wave model for undergraduates. *Eur. J. Phys.* **2019**, *40*, 025603. [CrossRef]
41. Buskirk, D.; Babiuc Hamilton, M.C. Eccentric pairs: Analytic gravitational waves from binary black holes in elliptic orbits. *Int. J. Mod. Phys. D* **2023**, *32*, 2250138. [CrossRef]
42. Huerta, E.A.; Kumar, P.; Agarwal, B.; George, D.; Schive, H.Y.; Pfeiffer, H.P.; Haas, R.; Ren, W.; Chu, T.; Boyle, M.; et al. Complete waveform model for compact binaries on eccentric orbits. *Phys. Rev. D* **2017**, *95*, 024038. [CrossRef]
43. McWilliams, S.T. Analytical Black-Hole Binary Merger Waveforms. *Phys. Rev. Lett.* **2019**, *122*, 191102. [CrossRef] [PubMed]
44. Boyle, M.; Hemberger, D.; Iozzo, D.A.B.; Lovelace, G.; Ossokine, S.; Pfeiffer, H.P.; Scheel, M.A.; Stein, L.C.; Woodford, C.J.; Zimmerman, A.B.; et al. The SXS collaboration catalog of binary black hole simulations. *Class. Quantum Gravity* **2019**, *36*, 195006. [CrossRef]
45. Foucart, F.; Duez, M.D.; Hinderer, T.; Caro, J.; Williamson, A.R.; Boyle, M.; Buonanno, A.; Haas, R.; Hemberger, D.A.; Kidder, L.E.; et al. Gravitational waveforms from SpEC simulations: Neutron star-neutron star and low-mass black hole-neutron star binaries. *Phys. Rev. D* **2019**, *99*, 044008. [CrossRef]
46. Blanchet, L. Post-Newtonian Theory and the Two-Body Problem. *arXiv* **2009**, arXiv:0907.3596.
47. Will, C.M. Inaugural Article: On the unreasonable effectiveness of the post-Newtonian approximation in gravitational physics. *Proc. Natl. Acad. Sci. USA* **2011**, *108*, 5938–5945. [CrossRef] [PubMed]
48. Blanchet, L. Gravitational Radiation from Post-Newtonian Sources and Inspiralling Compact Binaries. *Living Rev. Relativ.* **2014**, *17*, 2. [CrossRef] [PubMed]
49. Blanchet, L. Analyzing gravitational waves with general relativity. *C. R.—Phys.* **2019**, *20*, 507–520. [CrossRef]
50. Blackman, J.; Field, S.E.; Scheel, M.A.; Galley, C.R.; Ott, C.D.; Boyle, M.; Kidder, L.E.; Pfeiffer, H.P.; Szilágyi, B. Numerical relativity waveform surrogate model for generically precessing binary black hole mergers. *Phys. Rev. D* **2017**, *96*, 024058. [CrossRef]
51. Berti, E.; Cardoso, V.; Gonzalez, J.A.; Sperhake, U.; Hannam, M.; Husa, S.; Brügmann, B. Inspiral, merger, and ringdown of unequal mass black hole binaries: A multipolar analysis. *Phys. Rev. D* **2007**, *76*, 064034. [CrossRef]
52. Khanna, G.; Price, R.H. Black hole ringing, quasinormal modes, and light rings. *Phys. Rev. D* **2017**, *95*, 081501. [CrossRef]
53. Bambi, C. *Black Holes: A Laboratory for Testing Strong Gravity*; Springer: Berlin/Heidelberg, Germany, 2017. [CrossRef]
54. Buonanno, A.; Damour, T. Transition from inspiral to plunge in binary black hole coalescences. *Phys. Rev. D* **2000**, *62*, 064015. [CrossRef]
55. Berti, E.; Cardoso, V.; Starinets, A. TOPICAL REVIEW: Quasinormal modes of black holes and black branes. *Class. Quantum Gravity* **2009**, *26*, 163001. [CrossRef]
56. Berti, E.; Cardoso, V.; Will, C. Gravitational-wave spectroscopy of massive black holes with the space interferometer LISA. *Phys. Rev. D* **2006**, *73*, 064030. [CrossRef]
57. Rezzolla, L.; Diener, P.; Dorband, E.N.; Pollney, D.; Reisswig, C.; Schnetter, E.; Seiler, J. The Final Spin from the Coalescence of Aligned-Spin Black Hole Binaries. *Astrophys. J. Lett.* **2008**, *674*, L29. [CrossRef]
58. Barausse, E.; Rezzolla, L. Predicting the Direction of the Final Spin from the Coalescence of Two Black Holes. *Astrophys. J. Lett.* **2009**, *704*, L40–L44. [CrossRef]
59. Miller, J.M.; Miller, M.C.; Reynolds, C.S. The Angular Momenta of Neutron Stars and Black Holes as a Window on Supernovae. *Astrophys. J. Lett.* **2011**, *731*, L5. [CrossRef]
60. Lousto, C.O.; Zlochower, Y. Black hole binary remnant mass and spin: A new phenomenological formula. *Phys. Rev. D* **2014**, *89*, 104052. [CrossRef]
61. Shibata, M.; Hotokezaka, K. Merger and Mass Ejection of Neutron Star Binaries. *Annu. Rev. Nucl. Part. Sci.* **2019**, *69*, 41–64. [CrossRef]
62. Buskirk, D.; Babiuc Hamilton, M.C. Merging black holes: Assessing the performance of two analytic gravitational waves models. *J. Cosmol. Astropart. Phys.* **2023**, *2023*, 005. [CrossRef]
63. McNeil Forbes, M.; Bose, S.; Reddy, S.; Zhou, D.; Mukherjee, A.; De, S. Constraining the Neutron-Matter Equation of State with Gravitational Waves. *Phys. Rev. D* **2019**, *100*, 083010. [CrossRef]
64. Miller, M.C.; Chirenti, C.; Lamb, F.K. Constraining the Equation of State of High-density Cold Matter Using Nuclear and Astronomical Measurements. *Astrophys. J.* **2019**, *888*, 12. [CrossRef]
65. Flanagan, É.; Hinderer, T. Constraining neutron-star tidal Love numbers with gravitational-wave detectors. *Phys. Rev. D* **2008**, *77*, 021502. [CrossRef]
66. Damour, T.; Nagar, A.; Villain, L. Measurability of the tidal polarizability of neutron stars in late-inspiral gravitational-wave signals. *Phys. Rev. D* **2012**, *82*, 123007. [CrossRef]

67. Hinderer, T. Tidal Love Numbers of Neutron Stars. *Astrophys. J.* **2008**, *677*, 1216–1220. [CrossRef]
68. Zhao, T.; Lattimer, J.M. Tidal deformabilities and neutron star mergers. *Phys. Rev. D* **2018**, *98*, 063020. [CrossRef]
69. The LIGO Scientific Collaboration and the Virgo Collaboration. Properties of the Binary Neutron Star Merger GW170817. *Phys. Rev. X* **2019**, *9*, 011001.
70. Abac, A.; Dietrich, T.; Buonanno, A.; Steinhoff, J.; Ujevic, M. New and robust gravitational-waveform model for high-mass-ratio binary neutron star systems with dynamical tidal effects. *Phys. Rev. D* **2024**, *109*, 024062. [CrossRef]
71. Read, J.S.; Lackey, B.; Owen, B.; Friedman, J. Constraints on a phenomenologically parametrized neutron-star equation of state. *Phys. Rev. D* **2009**, *79*, 124032. [CrossRef]
72. Chatziioannou, K. Neutron-star tidal deformability and equation-of-state constraints. *Gen. Relativ. Gravit.* **2020**, *52*, 109. [CrossRef]
73. Bernuzzi, S.; Nagar, A.; Balmelli, S.; Dietrich, T.; Ujevic, M. Quasiuniversal Properties of Neutron Star Mergers. *Phys. Rev. Lett.* **2014**, *112*, 201101. [CrossRef]
74. Samajdar, A.; Dietrich, T. Waveform systematics for binary neutron star gravitational wave signals: Effects of the point-particle baseline and tidal descriptions. *Phys. Rev. D* **2018**, *98*, 124030. [CrossRef]